

Correcting Citizen-Science Air Temperature Measurements across the Netherlands for Shortwave Radiation Bias

Richard C. Cornes^{1,2*}, Marieke Dirksen¹, and Raymond Sluiter¹

¹*Royal Netherlands Meteorological Institute (KNMI), De Bilt, Netherlands*

²*Current affiliation: National Oceanography Centre, Southampton, UK*

**Corresponding author: richard.cornes@noc.ac.uk*

Abstract

Citizen-science thermometer measurements have the potential to provide information about surface air temperature fields on scales smaller than is typically quantified by the official monitoring network. As such National Meteorological Services are becoming increasingly interested in these measurements as a possible source of data for use in weather monitoring or forecasting. However, in order for the data to be used, biases in the data need to be assessed. The most important source of bias is the potential over-heating of the thermometer due to inadequate shielding or exposure. Previous research has indicated that information about the nature of the instrument and its exposure is important for correcting this bias. However, in the majority of cases this information is not available for amateur stations. In this paper we develop a statistical correction for shortwave radiation-bias in the air temperature data recorded at 159 Weather Observations Website (WOW) stations across the Netherlands during 2015 – 2016. Generalized Additive Mixed Modelling (GAMM) is used to quantify and correct for shortwave radiation bias in the hourly measurements, using a background temperature field generated from the official 34 automatic weather stations along with satellite-derived shortwave radiation estimates. It is demonstrated that the corrected WOW data add local detail to the hourly temperature field, which may provide a useful source of data to supplement official measurements.

Keywords: amateur observations; crowd sourced; Generalized Additive Model; Urban Heat Island; private weather stations

Running head: Citizen Science Temperature Measurements

Funder: KNMI "Meerjaren Strategisch Onderzoek (MSO)" project grant

29 1 Introduction

30 In 2011 the UK Met Office launched the Weather Observations Website (WOW) in associa-
31 tion with the Royal Meteorological Society (<https://wow.metoffice.gov.uk>). The project
32 aims to provide a web application through which individuals can upload their weather obser-
33 vations, recorded manually or via automatic weather stations, and access data recorded by
34 other observers. The repository contains both near-real time observations and historic ob-
35 servations from the WOW network. Although a relatively new venture, the WOW project
36 builds on earlier initiatives such as Weather Underground (www.wunderground.com), which
37 has provided web access to measurements recorded using private weather stations since 1993,
38 as well as projects that pre-date the internet age, notably the Climate Observers Link (COL)
39 (Brugge, 2010). The WOW network has grown substantially since its inception, with data
40 now being received from over 2000 sites worldwide, and associate projects have been de-
41 veloped in the Netherlands (WOW-NL, <https://wow.knmi.nl>) and Belgium (WOW-BE,
42 <https://wow.meteo.be>) by the Royal Netherlands Meteorological Institute (KNMI) and the
43 Royal Meteorological Institute of Belgium (KMI), respectively.

44 A particular advantage of the WOW and Weather Underground initiatives is the ability
45 to capture observations automatically from private weather stations. A range of variables
46 are recorded in the databases, including air temperature, wind speed and rainfall, and with
47 data uploaded as regularly as every ten minutes they constitute a large source of temporally
48 high-resolution readings (Bell et al., 2013). Given the wealth of observations in the WOW
49 repository, there has been a great deal of interest in the potential use of these data by Na-
50 tional Meteorological Services for weather monitoring and forecasting (Krennert et al., 2018).
51 In contrast to the locations of World Meteorological Organization (WMO) approved official
52 weather stations, which aim to provide measurements that are representative over a wide area,
53 amateur stations are mostly sited in populated areas, and as such may provide important local
54 weather information, particularly in relation to urban environments (Wolters and Brandsma,
55 2012; Bell et al., 2013; Muller et al., 2013; Chapman et al., 2017; Fenner et al., 2017; Meier
56 et al., 2017; de Vos et al., 2017; Napoly et al., 2018).

57 In the Netherlands, there has been considerable research interest in the use of non-standard
58 meteorological measurements to supplement the network of official measurements. These have

59 ranged from weather stations attached to lampposts (Ronda et al., 2017) to the amateur
60 measurements that are contained in the Weather Underground database (Steenefeld et al.,
61 2011; Wolters and Brandsma, 2012). Despite the different types of instruments used, all of
62 the studies have sought to use the measurements to analyse urban meteorology, and especially
63 to improve knowledge about the Urban Heat Island (UHI) effect (Oke, 1982; Chapman et al.,
64 2017; Steenefeld et al., 2011; Theeuwes et al., 2016; Thorsson et al., 2014; Lindberg and
65 Grimmond, 2011). This is a particularly important field of research given the increasing
66 proportion of urbanization in the country (DESA, 2017) along with the projected increase in
67 heatwaves in future decades (van den Hurk et al., 2006; Haines et al., 2006) — the effects
68 of which are potentially amplified by the UHI (Heusinkveld et al., 2010, 2014; Li and Bou-
69 Zeid, 2013; Li et al., 2015; Zhao et al., 2018), and are associated with an increase in thermal
70 discomfort (Molenaar et al., 2016).

71 The thermometer observations contained in the WOW repository can potentially provide
72 useful information about urban temperature but in order to fully utilise this information the
73 data must be corrected for potential biases. The siting of the instruments as well as the
74 type of instruments used can introduce biases that exceed the manufacturer-stated tolerances.
75 This was demonstrated in the year-long test of several commonly used amateur meteorological
76 stations alongside the official UK Met Office measurements at the Winterbourne meteorological
77 enclosure in Edgbaston, Birmingham by Bell (2014) and Bell et al. (2015). The air temperature
78 measurements displayed a marked bias as a result of inadequate radiation shielding — a feature
79 that has also been noted by Jenkins (2014) and Meier et al. (2017)— although the severity of
80 this bias was dependent on the type of instrument used. Using this information, a statistical
81 approach was developed by Bell (2014) to correct for radiation bias, along with the likely bias
82 introduced from poor instrument calibration.

83 In this paper we analyse the hourly, near-surface air temperature data recorded at WOW
84 sites across the Netherlands during the 24-month period from January 2015 until December
85 2016. These data have not previously been assessed for radiation bias in a systematic way.
86 Taking the findings of the previous studies described above as a starting point, we derive a
87 station-by-station correction for the WOW data using a statistical model that takes into ac-
88 count the background temperature field (derived from the official temperature measurements),
89 and an estimate of local direct shortwave radiation obtained from satellite data. We demon-

90 strate that the corrected WOW data add local detail to the hourly temperature field, which
91 may provide a useful source of data to supplement official measurements.

92 **2 Data and Methods**

93 **2.1 The nature of the WOW temperature data**

94 The WOW air temperature data for stations situated in the Netherlands were obtained from
95 the UK Met Office data repository, along with the latitude/longitude coordinates of the station
96 and the time of observation. The number of WOW stations covering the Netherlands marks a
97 substantial increase over the number of official sites. During the period 2015–2016 a total of
98 318 stations supplied data to the WOW database, compared to the 34 official weather stations
99 (Figure 1). However, not all of the WOW station series are complete for this period and
100 stations were only used if they supplied (interpolated) hourly values that were 80 % complete
101 for each month. This resulted in a sample of 159 stations for use in this analysis. It should
102 be noted that the official KNMI automatic weather station (AWS) data are now included in
103 the WOW database, and when referring to the WOW stations we have excluded the AWS
104 stations.

105 The WOW stations are generally situated in urban environments, often in people’s gardens
106 or on school premises. The instruments typically used are relatively low-cost and are manufac-
107 tured, for example, by Davis Instruments or Oregon Scientific (Bell et al., 2015), although the
108 instruments from other manufacturers may be used as there is no stipulation on instrument-
109 type for the entry of data to the WOW. In addition, while there is the ability for observers
110 to supply meta-data in a standardized format, this is not mandatory; Bell (2014) estimated
111 that 15 % of observers omit this information, and clear information about the hardware used
112 was available in only around 60 % of stations. The coordinates of the station are mandatory
113 information, although the station altitude is not required; Bell (2014) estimated that for the
114 UK this altitude information was supplied by fewer than 75 % of observers.

115 In this analysis, all of the 159 WOW stations were analysed. However, four sample stations
116 were selected for closer examination. These stations represent the range of instruments and
117 exposure of the network across the Netherlands; the properties of these stations are summa-
118 rized in Table 1. Site A is a high-quality instrument situated in the De Bilt official WMO

119 meteorological enclosure close to the official temperature measurements. Site B is a typical
120 instrument sited in a sheltered suburban garden. Site C uses the same instrument as Site B,
121 but is located in a low-cut grass field with an open exposure, where the nearest building is
122 10m from the weather station. Site D has a standard residential exposure and is situated in
123 the east of the country; the station uses the relatively low-cost AcuRite 5 in 1 instrument.

124 The WOW observations are recorded on varying time scales. In this analysis we are only
125 interested in hourly values and in order to simplify the analysis, the observation times were
126 rounded to the nearest 10 minute and these values were then interpolated to regular hours by
127 fitting a cubic smoothing spline to each station series. Gaps of longer than two hours (in the
128 10-minute values) without an observation were marked as missing.

129 2.2 The correction model

130 Generalized Additive Modelling (GAM) was used as the basis for the correction of the WOW
131 data. GAMs are an extension of Generalized Linear Modelling (GLM), which themselves are
132 a more flexible version of ordinary-least-squares regression, and allow a model to be fitted to a
133 dependent variable that is not necessarily from a Gaussian distribution (Hastie and Tibshirani,
134 1990). GAMs extend GLMs by allowing the use of one or more unknown (smooth) functions,
135 and may also include linear coefficients. Generalized Additive Mixed Modelling (GAMM) is a
136 further development that allows random effects and correlation structures to be accommodated
137 in the model (Wood, 2006).

138 Using the findings of Bell (2014) as a basis we modelled the WOW station data (T_{wow} with
139 outcome at time i) at each site under a semi-parametric scheme (Hastie and Tibshirani, 1990)
140 using shortwave radiation (Rad) and background temperature (T_{bg}) terms as

$$T_{wow,i} = \beta_0 + \beta_1(Rad_i) + f(T_{bg,i}) + \epsilon_i, \quad \epsilon_i = \phi_i \epsilon_{i-2} + v_i,$$

141 where T_{bg} is formed from an interpolation of the hourly temperature measurements recorded
142 at the official KNMI weather stations, and Rad is formed from a local estimate of incoming so-
143 lar radiation derived from satellite retrievals. β_0 represents an intercept term, and ϵ is random
144 error assumed to be identically and independently distributed (i.i.d). Rad values represent
145 hourly averages over the hour leading up to the temperature observation. This corresponds

146 to the findings of Bell (2014) who demonstrated a 1-2 hour lagged response of the WOW
147 measurements to shortwave radiation at the Winterbourne test site. In contrast, T_{bg} represent
148 estimates of concurrent temperature measurements. The local derivation of Rad and T_{bg} is
149 described below

150 The smooth function f can be derived in a number of ways. Since we are dealing with a
151 univariate function the piece-wise cubic polynomial spline is an obvious choice as it is relatively
152 quick to converge. However, better model fitting was achieved by using a Thin-Plate Regression
153 Spline (TPRS) (Wood, 2003). TPRS are a more general form of cubic splines, and in practice
154 with the data used here produced splines that were slightly smoother and which were more
155 physically plausible.

156 Since the WOW observations analysed in this paper are comprised of hourly observations,
157 temporal autocorrelation in the observations needs to be taken into account in the models
158 in order to satisfy the i.i.d assumption. Neglecting temporal autocorrelation may lead to
159 inaccurate parameter estimation and poor uncertainty estimates of the model terms (Wood,
160 2006). We used a lag-2 autoregressive model in the GAMM, where the autoregressive coefficient
161 (ϕ) is estimated as part of the model fitting. The autoregressive function was nested in each
162 month of data in order to speed-up the calculation. A variety of lag intervals were tested
163 and the lag-2 autocorrelation model effectively counteracted temporal autocorrelation in ϵ , up
164 to a lag of 10 hours. A low-level of autocorrelation at around lag-24 remained in ϵ for many
165 stations. This appears to represent a local diurnal cycle not quantified in the model covariates,
166 and is a likely feature of the local temperature data.

167 In this model the form of each of the parameters is chosen via a backfitting algorithm that
168 iteratively selects an optimal fitting of each function. The fitting of the smooth function f
169 represents a balance between over- and under-fitting of the function, i.e. between a spline
170 that is too smooth and one that is too “wiggly”. A penalization is imposed to the function
171 f to avoid over-fitting of the spline. An optimal fitting of the function in these models is
172 obtained through the calculation of a score that measures the degree to which the predictive
173 error is minimised. In the WOW-correction models used in this paper Marginal Likelihood
174 (ML) scores are used.

175 The fitting of the smoothed terms in the models used in this paper rely on the prior
176 setting of an upper limit (k) on the effective degrees of freedom (EDF) of the smoothing terms

177 (Wood, 2003). This allows for a more efficient way of fitting the smoothing functions through
 178 an eigendecomposition, but necessitates the subjective selection of k . As stressed by Wood
 179 (2006) however, while this selection of k is subjective, the actual selection of the EDF uses the
 180 pre-selected optimization procedure (Marginal Likelihood in this case), up to a limit of $k - 1$.
 181 Values of $k = 30$ were chosen for the models used in this paper following application of the
 182 heuristic tests recommended by Wood (2006).

183 This model assumes that $T_{wow,i}$ can be modelled as a non-linear response to $T_{bg,i}$ (via f)
 184 plus a linear response to Rad_i (via the coefficient β_1). By making this assumption we are able
 185 to ensure that the response to radiation scales from a partial intercept at zero. We also tested
 186 whether a simple model where the response to T_{bg} was also linear, i.e. in the form of a GLM.
 187 A significant difference was observed in these models in terms of the explained variance and
 188 we therefore opted to retain the use of the smoothing function f under the GAMM scheme.
 189 The non-linearity in f represents the local distortion to the background temperature field that
 190 is assumed to arise from the temperature environment of the WOW station.

191 Prior to model-fitting, the T_{wow} values were quality-controlled against the respective T_{bg}
 192 values: $|T_{wow} - T_{bg}| > 8^\circ C$ values were removed, and identical values of T_{wow} for more than
 193 four consecutive hours were excluded. The Urban Heat Island in cities across the Netherlands
 194 has been estimated by Steeneveld et al. (2011) to be of the order of $6^\circ C$ during calm, fair
 195 weather and hence the threshold of $8^\circ C$ does not preclude the capturing of these types of
 196 features in the data.

197 Since the GAM(M)s are additive in nature, the partial effects of each of the covariates
 198 can be assessed individually. Specifically, the contribution of the shortwave radiation term
 199 $\beta_1(Rad)$ may be extracted from the WOW temperature data as

$$T'_{wow,i} = T_{wow,i} - \beta_1(Rad_i)$$

200 to produce the corrected WOW values ($T'_{wow,i}$). In this way the shortwave radiation effect,
 201 as modelled by the partial regression coefficient β_1 , is removed from T_{wow} , and the corrected
 202 temperature values are obtained from the (non-linear) relationship to T_{bg} (estimated from
 203 f) plus any residual effect contained in ϵ . Although the correction is zero at nighttime, the
 204 models were applied to the data over the full 24-hour period to increase the sample size for

205 fitting of the function $f(T_{bg})$. Since the correction is applied through $\beta_1(Rad)$, this correction
206 should be viewed as a parameterization of the shortwave radiation effect at a given WOW
207 station, under the assumption that any shortwave radiation effect detected in the data is an
208 artificial bias that results from inadequate shielding or siting of the instrument.

209 **2.3 The background temperature field (T_{bg})**

210 The background temperature values (T_{bg}) were calculated by fitting a GAM to the temper-
211 ature measurements recorded at the 34 official KNMI AWS sites (Figure 1), which was then
212 interpolated to the WOW station locations. In this case a tensive spline was used to model
213 the three-dimensional interaction of temperature across space (using longitude and latitude
214 coordinates) and time:

$$T_{bg,i} = \beta_0 + f(lon_i, lat_i, time_i) + \epsilon_i.$$

215 This space-time model is preferable to more common spatial interpolation techniques such
216 as kriging — which typically use only spatial coordinates and construct separate models for
217 each time-step — as the sample size for model fitting is increased considerably. This is im-
218 portant as there are only 34 AWS stations across the Netherlands, and this represents a small
219 sample size for fitting the interpolating model. The tensive spline has the advantage of being
220 insensitive to the units of measurement of the covariates (Wood, 2006), (degrees in the case
221 of longitude and latitude, and hours in the case of time). The spline is formed using the joint
222 interaction of longitude/latitude and time, where both components take a thin-plate spline
223 basis. As such an anisotropic relationship over space is modelled. The temperature lapse rate
224 is best captured by the longitude/latitude coordinates, since the altitude is relatively constant
225 across the Netherlands and for these purposes only becomes significant across the south of
226 the country. Tests were carried out using altitude as an additional covariate. However, the
227 fitted function did not have a plausible physical interpretation, which likely resulted from the
228 masking of the lapse-rate by hourly-scale temperature variations. Furthermore, altitude values
229 are not supplied in the WOW-station metadata and would need to be estimated via a Digital
230 Elevation Model adding to the uncertainty in lapse-rate estimation. Three other environmen-
231 tal parameters (coastal proximity, slope and aspect) were also tested in this model but were

232 found to be insignificant, and are most likely also accommodated by the joint-interaction of
233 the latitude and longitude components.

234 It is impractical to fit this background temperature model to all of the data points simul-
235 taneously, since the model would take a considerable length of time and significant computing
236 resources to converge. Therefore the model was fitted on a day-by-day basis. To limit the
237 occurrence of edge effects, an overlap of six hours was used and hence for a given day data
238 from 6pm UTC of the previous day to 6AM UTC of the following day were used to produce
239 a moving-window of overlapping models.

240 **2.4 The local shortwave radiation data (*Rad*)**

241 Estimates of global solar radiation (the sum of direct and diffuse radiation) at the WOW sites
242 are derived from the MSG-CPP dataset (www.msgcpp.knmi.nl). These values are calculated
243 from the Meteosat SEVIRI imagery using the KNMI Cloud Physical Properties (CPP) al-
244 gorithm (Roebeling et al., 2006). In the visible range of the spectrum this dataset provides
245 15-minute retrievals at a ca. 1km resolution. At each WOW station the surface downwelling
246 shortwave (SDS) radiation values (in the unit of W/m^2) were calculated as the average of the
247 nearest 3x3 pixels after Greuell et al. (2013).

248 The CPP algorithm calculates the SDS values using cloud retrievals and satellite-derived
249 reflectances. Deneke et al. (2008) evaluated the shortwave radiation data obtained from the
250 MSG-CPP dataset over the Netherlands through a comparison against pyranometer measure-
251 ments recorded at the official KNMI stations. They found that surface irradiance values were
252 comparable to ground-based instruments in the summer, although during the winter the ac-
253 curacy was lower as a result of the low sun elevation in combination with the large satellite
254 viewing angle across the Netherlands. Hence the data are considered to be suitable for the
255 correction of the WOW data, which are generally only affected by shortwave radiation bias at
256 higher radiation values, as indicated by the linear scaling against the radiation values from a
257 zero intercept. Night-time values (missing in the MSG-CPP visible spectrum data) were set
258 to zero.

259 3 Results and Discussion

260 3.1 The background temperature and radiation values

261 Reliable estimations of the background temperature (T_{bg}) and shortwave radiation values
262 (Rad) at each of the WOW sites are essential for successfully modelling, and ultimately cor-
263 recting, the WOW temperature measurements as any deficiency would potentially produce
264 skewed model residuals that would violate the i.i.d assumption of the model. To provide an
265 indication of the reliability of the background temperature model a leave-one-out cross vali-
266 dation exercise was conducted, using the observations from the official 34 official AWS (see
267 Figure 1). This exercise consisted of removing one AWS station at a time and interpolating
268 to that candidate station over all time steps in the years 2015–16 using the data from the
269 remaining stations. This cross-validation was repeated for each AWS in turn. The error of
270 T_{bg} relative to the official measurements was then calculated, with the assumption being that
271 a similar degree of error relative to T_{bg} would also be applicable to the WOW stations. The
272 results indicate that the interpolation produces a broadly unbiased estimate of the local tem-
273 perature (Figure 2). Root-mean squared error (RMSE) values for most stations are in the
274 range 0.4–0.8 °C, although there is a degree of variation during different seasons, with higher
275 RMSE values at certain stations during spring, summer and autumn. The largest of these
276 values (RMSE > 1.5 °C) occur at the border regions, and likely result from the relatively large
277 distances from the nearest stations. Improvements could be made by incorporating data from
278 neighbouring countries.

279 The degree of error indicated in this cross-validation exercise compares favourably with the
280 results obtained by Bell (2014). That study similarly constructed background temperature
281 fields for the correction of UK-based WOW temperature readings. However, the method used
282 to interpolate the official measurements in the present study is greatly simplified compared to
283 the fields constructed by Bell (2014), which included many more covariates. The atmospheric
284 environment of the Netherlands does not require the range of covariates that are necessary for
285 an interpolation of temperature across the UK, but also the tensive spline used here provides
286 a more optimal fit of the data, using the few covariates that are employed. Notably, we do not
287 include short-range weather forecast data as a covariate in the model, as was the case with Bell
288 (2014), since a potential application of these data is assimilation in numerical weather models,

289 and including the corrected WOW data could confound the determination of local temperature
290 information afforded by the WOW data. The GAMs are, however, flexible enough to allow
291 incorporation of such variables as additional model terms if required in future extensions of
292 the method.

293 The reliability of the local shortwave radiation estimates (*Rad*) were assessed by evaluating
294 the MSG-CPP values against surface shortwave radiation values recorded at each of the official
295 weather stations. The MSG-CPP radiation estimates are strongly linearly related with station-
296 based shortwave radiation measurements during the year 2015–2016 (Figure 3), and have a
297 small bias of -2.29 W/m^2 and a RMSE value of 36.93 W/m^2 . These values are in accordance
298 with the findings of Deneke et al. (2008).

299 **3.2 Evaluation of the GAMM for Station B**

300 A GAMM was developed for each of the selected 159 WOW stations, following the method
301 described in Section 2, using data for the years 2015 and 2016. To provide an example of
302 the nature of the statistical models and the radiation correction, the results for station B (see
303 Table 1) are evaluated in this section.

304 The statistical model for Station B explains 98 % of the variation in the hourly WOW
305 temperature data (Figure 4 a), and the residuals from the model are normally distributed
306 with a standard deviation of $0.9 \text{ }^\circ\text{C}$ (Figure 4 b). This indicates that the WOW temperature
307 measurements can be successfully modelled using the background temperature and shortwave
308 radiation parameters since a deficiency in the model, for example through an important miss-
309 ing parameter, would produce a skewed distribution in the residuals. The incorporation of
310 the autocorrelation factor into the model has significantly reduced the degree of temporal
311 autocorrelation in the model’s residual. This is demonstrated in Figure 4 c, where residual au-
312 tocorrelation up to a lag of 41 hours from the lag-2 model are compared against those derived
313 where no temporal autocorrelation is assumed. The residual autocorrelation is reduced at all
314 lag intervals, particularly at lag-1. This plot also displays a moderate degree of autocorrela-
315 tion at around a lag of 24 hours, which indicates that the model is failing to capture a diurnal
316 cycle in the WOW temperature values. This may be a result of an inadequate representation
317 of heating from solar radiation, or may be a true feature of the local temperature field that
318 represents a diurnal urban temperature cycle.

319 In the model for this station both of the parameters [$f(T_{bg})$ and $\beta_1(Rad)$] are highly
320 significant predictors ($p < 0.001$). A strong relationship with T_{bg} is to be expected, however the
321 importance of Rad as a predictor is used as an indication of significant shortwave radiation
322 bias in the WOW readings for this station. In Figures 4 d and e the partial model terms are
323 plotted. It should be notated that the model-fitting is applied to values of y expressed as
324 deviations from the mean of y and hence in those figures the temperature response values are
325 relative to the intercept (β_0). The function $f(T_{bg})$ with 13 degrees of freedom shows a non-
326 linear relationship to the background temperature, with the largest deviations from linearity
327 occurring at the lowest temperature values. The radiation coefficient term ($\beta_1 = 2.09e - 03$)
328 scales from zero to a value of $1.67 \text{ }^\circ\text{C}$ ($\pm 0.09 \text{ }^\circ\text{C}$, 95 % confidence interval) at $Rad = 800\text{W}/\text{m}^2$.

329 Since the statistical models used here are additive in nature, the original time series of
330 WOW values can be decomposed into each of the model terms. The results from the time
331 series decomposition for Station B are demonstrated in Figure 5 for the year 2016. It should
332 be noted when evaluating this figure that the sum of the background temperature component,
333 shortwave radiation component, residual and the model intercept, equal the raw WOW values.
334 The annual and diurnal cycles in the shortwave radiation component are readily apparent from
335 this figure.

336 The magnitude of the estimated shortwave radiation bias in Station B is much larger than
337 that measured using a similar instrument (Davis *Vantage Pro 2*) by Bell (2014) in the field-
338 test at the Winterbourne meteorological enclosure; that instrument showed no appreciable
339 radiation bias. However, the instrument used in that experiment was equipped with fan-
340 assisted aspiration, whereas the instrument at used at Station B is naturally ventilated; the
341 lack of assisted ventilation therefore appears to have a detectable effect in these results and
342 leads to significant over-heating under moderate-to-high levels of insolation ($>500 \text{ W}/\text{m}^2$).

343 **3.3 Evaluation of the Radiation Bias in all Test Stations**

344 In Figure 6, tile plots are produced for the four Test Stations (Table 1). These plots show
345 the average bias per month and per hour of the day (c.f similar plots by (Bell et al., 2015) for
346 the Winterbourne test site). Stations A and C have the lowest estimated shortwave radiation
347 bias, up to average values of $0.6\text{--}0.7 \text{ }^\circ\text{C}$ in the summer months at around noon. Since Site
348 A uses a high-quality instrument and is sited in the official De Bilt Meteorological enclosure,

349 a relatively low bias would be expected. The results from Site D show the largest bias, with
350 average noon biases reaching values above 3 °C during high-summer.

351 Sites B and C both use a passively-ventilated Davis Vantage Pro2 instrument. The main
352 difference in these sites is the exposure of the instruments: the instrument at Site C is sited
353 in an open field that consists of short grass, whereas Site B is in a more enclosed residential
354 setting. These results therefore suggest that the increased air-flow that would be expected
355 at Site C enhances the passive ventilation and reduces the shortwave-radiation bias in the
356 temperature readings. This effect could possibly be incorporated into the statistical models
357 through the incorporation of wind speed as an additional covariate. However, while many
358 stations record wind speed, it is not ubiquitous across the network and the values are highly
359 susceptible to local wind-flow distortion. Nonetheless, incorporation of this parameter in the
360 models could be considered in future updates to the method.

361 Since Station A is located in the De Bilt meteorological enclosure the validity of the
362 radiation correction can be assessed through comparing the WOW data against the official
363 AWS temperature measurements. In Figure 7 we have plotted the root-mean squared error of
364 the raw and corrected WOW data relative to the AWS data for at each hour of the day for four
365 selected months. The correction to the data has reduced the error to values consistent with
366 those observed during the night, when no corrections are applied to the data. This background
367 level of error is the same order of magnitude as the precision of the measurements that has been
368 estimated by the instrument manufacturer to be between ± 0.3 – 0.4 °C. Variations around this
369 range in the corrected readings in Figure 7 likely result from sampling bias, arising from the
370 relatively small sample sizes used here and because the errors are not taken under laboratory
371 conditions.

372 **3.4 Correcting Shortwave Radiation Bias across the WOW network**

373 To examine the T_{bg} and Rad responses across the network, we have plotted the partial model
374 terms for all of the selected 159 WOW stations in Figure 8, in a similar manner to Figures
375 4 d and e above; the terms for the four test stations are also indicated. The departure from
376 linearity of the T_{bg} terms is most evident at the lower temperature values, and is apparent
377 in many of the stations. This non-linearity is likely a result of the urban distortion to the
378 background temperature field, beyond the shortwave radiation effect that is captured by the

379 term $\beta_1(Rad)$.

380 The radiation coefficient (β_1) is significant in all of the station models. However, the
381 magnitude of bias estimated using this coefficient varies greatly across the network (Figure 8
382 b). Several stations have radiation bias that is below 0.3 °C across the range of radiation values,
383 and this is below the usual manufacturer-stated precision that is typically of the order of ± 0.3
384 °C. Other stations have large estimated bias that are exceed 2 °C at $Rad = 800 \text{ W/m}^2$. It is
385 likely that the range of β_1 coefficients across the network results from the different instruments
386 employed. This cannot be verified as the meta-data for all stations are not easy to acquire
387 (c.f. Bell (2014) who used 'web-scraping' to obtain information for certain UK WOW stations),
388 however the results from the four test stations — for which we do know the type of instruments
389 used and their general situation — suggest that this is the case. Test stations A and C are
390 at the lower range of this spread, whereas Station D is the station that is most affected by
391 shortwave radiation bias by this estimation. However, as suggested above, it would seem
392 that the degree of shortwave radiation effect is a combination of the nature of the instrument
393 and the exposure/situation of the instrument. In addition to the enhanced ventilation in the
394 Davis VP2 instruments, these siting-effects likely also include a myriad of factors such as the
395 sky-view factor, the local land-use or local boundary conditions. An evaluation of a network
396 of sensors such as that provided Netatmo (e.g. Napoly et al. (2018)) would be useful in this
397 respect, since the confounding effect of different instrument types would be removed.

398 Several previous studies have indicated a non-linear response of citizen-science temperature
399 observations to shortwave radiation bias (Jenkins, 2014), particularly for those instruments
400 that were particularly vulnerable to shortwave radiation bias (Bell, 2014). A linear function
401 was used in the GAMMs developed in the present study in order to ensure a scaling of the
402 radiation component from a partial zero intercept, but this is likely to be a simplification. The
403 analysis by Bell (2014) indicated that a quadratic function was most suitable for capturing
404 the radiation effect in the stations most affected by such biases, and hence the linear function
405 used here is likely to be a conservative estimate of shortwave radiation bias.

406 One of the main applications of the WOW data is for the examination of the UHI effect,
407 which is generally not captured by the official network of weather stations. A risk with the
408 correcting of the WOW station temperature data is that true UHI is mistaken for shortwave
409 radiation bias. To examine this we have calculated the diurnal cycle of temperature for each

410 season as averages from the official AWS data and both the raw and corrected WOW tem-
411 perature measurements (Figure 9). The results indicate a typical feature found in the diurnal
412 temperature cycle of urban areas relative to the background rural temperature (represented
413 here by the AWS data) (Oke et al., 2017). Temperatures during the night are generally warmer
414 in urban areas but around dawn this difference reduces. This remains the case until the af-
415 ternoon when the difference increases again. The corrected WOW values in Figure 9 clearly
416 show this diurnal variation. In contrast, the raw WOW values show an augmented diurnal
417 cycle with elevated temperatures between around 9–14UTC, particularly during the spring
418 and summer seasons. These results indicate that while the largest shortwave radiation bias
419 is removed from the data, the urban-related diurnal cycle is retained in the corrected WOW
420 data.

421 **3.5 Mapping the Temperature Data**

422 To assess the value of the corrected WOW temperatures in examining the temperature field
423 across the Netherlands, we have mapped the AWS temperature values and the AWS together
424 with the corrected WOW data maps (AWS+WOW). This has been done for the hottest and
425 coldest events in the Netherlands during the 2015–2016 period: the 1300UTC readings from
426 2 July 2015, and the 0300UTC readings from 19 January 2016 (Figure 10). By comparing
427 the AWS and AWS+WOW maps the extra detail added by the WOW data can be examined.
428 It should be noted, however, that while the AWS are relatively evenly spatially distributed
429 the WOW are concentrated in urban areas and hence the AWS+WOW interpolation will be
430 biased towards the urban areas.

431 The July 2015 event was connected with a southerly airflow resulting from a high-pressure
432 system centred over Scandinavia, and occurred during a week that saw very high temperatures
433 recorded across northwest Europe. The spatial pattern of temperature observed from the AWS
434 and AWS+WOW stations is broadly similar, with a gradient of temperatures evident across
435 the country from 36 °C in the south to less than 24 °C at the coast. However, the map
436 calculated using the AWS+WOW data indicates local detail not seen in the maps generated
437 from the AWS data alone. In particular, several urban heat and cool islands (Oke et al., 2017)
438 are apparent in the data, which correspond to urban centres and parkland respectively.

439 The January 2016 event was associated with the development of a ridge of high-pressure

440 that had built from the east over the previous two days. As with the July 2015 maps, the
441 spatial gradient is broadly consistent in the maps produced from the AWS and AWS+WOW
442 data, although additional spatial features are apparent in the maps using the AWS+WOW
443 data. Temperatures are on the whole are warmer in the AWS+WOW map, which likely reflects
444 the urban-bias in the location of the WOW stations. A relatively large difference also occurs
445 in the south-western extremity of the country. The nearest official AWS at the location is at
446 Vlissingen, which although located on land is significantly affected by oceanic conditions. The
447 use of the corrected WOW data result in a cooler interpolated temperature for that region,
448 which further indicates the warm bias at the Vlissingen site during this cold winter event.

449 A factor that is not taken in correction of the WOW temperature data is the spatial-scale
450 lengths that are represented by the WOW data. The AWS locations are chosen so that the
451 data are representative of conditions over a relatively wide area, although as discussed above in
452 the case of certain stations such as Vlissingen this ideal may not always be reached. Similarly,
453 the WOW stations should be representative of the general conditions that are experienced in
454 the vicinity of the station, albeit in this case often from an urban environment. In practice,
455 however, the stations are sited at the convenience of the observer and hence the readings
456 will represent a very small area (Bell, 2014), possibly on the scale of a few metres. This
457 need not be the case, however, as indicated in the case of sample station C (see Table 1),
458 which appear to represent well the conditions surrounding the observation-site on account of
459 the instrument being located in an open situation, which is typical of the local environment.
460 Nonetheless, in order to make full use of the (corrected) WOW data for examining temperature
461 fields an evaluation of the likely spatial scale represented by each of the station would need
462 to be conducted. This would entail an examination of the surrounding environment of the
463 station, through the use of digital terrain information. This would also require precise station
464 coordinates, which are not always provided. However, representativity error could be reduced
465 when using the WOW data (in combination with the official AWS data) for country-scale
466 mapping through a spatial smoothing procedure. The degree of smoothing used in Figure
467 10, for example, is determined by the nugget variance of the variograms, which is estimated
468 automatically. Hence the maps calculated from the AWS+WOW data depict a spatial-scale
469 that is larger than the station-scale but smaller than the AWS maps. However, these maps
470 are not able to detect all features of urban temperature, given the large intra-urban variability

471 in air temperature.

472 **3.6 Aspects to Consider for Operational use of the Corrected Data**

473 The WOW data are uploaded by users in near-realtime, with often only a delay of minutes
474 before the data are made available on the WOW website. Similarly, both the satellite data and
475 the AWS values are available in near-realtime. The WOW data and this correction method
476 are therefore of potential use in operational observing or forecasting procedures by National
477 Meteorological Services. The question therefore arises: how can the GAMM approach to
478 correcting the WOW temperature data developed in this paper be used in such operational
479 situations?

480 A major limitation to the use of the WOW data is the short duration of many records. In
481 this analysis only around half of the total stations that supplied data to the WOW repository
482 during the period 2015–2016 were used, since criteria were placed on the minimum number
483 of missing values in a series (see Section 2.1). While this ensures that the statistical models
484 are comparable between stations, it severely limits the pool of available stations. A different
485 approach was taken by Bell (2014). His analysis used an algorithm that gradually adjusted
486 the uncertainty of the bias as new data were added. Such an approach could be used in the
487 GAMM models presented here through use of the standard error metrics that can be calculated
488 for the smoothing splines (see for example Figure 4 e). These uncertainty estimates would
489 be expected to reflect sampling density, and could be used to indicate uncertainty through a
490 resampling scheme, through which draws from the posterior distribution of the spline could
491 be taken; these values could be used to produce a range of plausible corrections relative to the
492 spline uncertainty.

493 The question also arises in an operational setting about the speed of computation. The
494 GAMM takes considerable time to converge (several hours for a given station). However, in an
495 operational context a given model could be saved for each station and the corrections applied
496 as new data are received. The background temperature values are quicker to derive since
497 an autocorrelation is not embedded in the model. Similarly the satellite-derived shortwave
498 radiation estimates are quick to produce, since their derivation only relies on a pixel-overlay
499 across the station network.

500 4 Conclusions

501 A correction for shortwave radiation-bias has been calculated for the hourly temperature mea-
502 surements taken at 159 WOW sites across the Netherlands. The corrections were derived on a
503 station-by-station basis for data recorded over the 2015–2016 period, with the aim of retaining
504 the local-scale information contained within the data, whilst removing the bias resulting from
505 inadequate shortwave radiation shielding. Although derived for the WOW network across the
506 Netherlands, the technique developed in this paper could equally be applied to other stations
507 in the WOW network — which has the highest density across the UK, the Netherlands and
508 Belgium – and to other platforms such as Weather Underground or Netatmo, which offer a
509 wider area of investigation.

510 The correction is calculated by fitting a Generalized Additive Mixed Model (GAMM) to
511 each station series, using satellite-derived shortwave radiation estimates and a local estimate
512 of the background temperature as model covariates. By decomposing the WOW temperature
513 series into components relating to each of the covariates, the effects of the shortwave radiation
514 component can be extracted from the data. The GAMM-approach offers an extremely flexible
515 way of modelling and hence correcting the WOW data, through the ability to model both
516 linear and non-linear responses and to incorporate a temporal autocorrelation component.

517 We have focused on shortwave radiation-bias in this paper, as this the most significant
518 limitation that is expected in readings from relatively low-cost weather stations, and which
519 through necessity are generally not sited in optimal locations. The shortwave radiation biases
520 estimated through the models developed in this paper are broadly comparable in magnitude
521 to those measured or estimated in previous analyses. However, these models are able to
522 correct for the shortwave radiation bias in the absence of meta-data about the nature of
523 the instruments or their exposure – information that is typically missing or incomplete in
524 databases of citizen-science observations. The correction relies on the assumption that any
525 direct relationship between global shortwave radiation and temperature values beyond the
526 background (rural) temperature temperatures are due to shortwave radiation-bias. Under
527 this assumption shortwave radiation biases are detected in all of the WOW stations but the
528 magnitude of bias varies considerably across the network. This appears to be related to a
529 combination of the nature of the instruments and their exposure. Further analysis is required

530 on the spatial-scale that is depicted in the corrected WOW data. Nonetheless, the data
531 potentially allow a more detailed picture to be developed about temperature variability at a
532 scale smaller than can be depicted by the official network of instruments, and particularly with
533 regard to urban effects on the temperature field.

534 **Acknowledgements**

535 We are grateful to the UK Met Office for maintaining the WOW network ([https://www.
536 metoffice.gov.uk/nl](https://www.metoffice.gov.uk/nl)), and to all of the observers who supply data to the network. The
537 authors would like to thank Jake Brown and Katharine O’Boyle (Met Office) for extracting
538 the WOW data, Reinout Boers (KNMI) for constructive criticism of the manuscript and Remie
539 van Bommel for providing details about Test Station C. This research was funded by a KNMI
540 “Meerjaren Strategisch Onderzoek (MSO)” project grant. The models developed in this paper
541 were produced using the *mgcv* package for R (Wood, 2018).

542 **References**

- 543 Bell, S. (2014). *Quantifying Uncertainty in Citizen Weather Data*. PhD thesis, Aston Univer-
544 sity.
- 545 Bell, S., Cornford, D., and Bastin, L. (2013). The state of automated amateur weather
546 observations. *Weather*, 68(2):36–41.
- 547 Bell, S., Cornford, D., and Bastin, L. (2015). How good are citizen weather stations? Ad-
548 dressing a biased opinion. *Weather*, 70(3):75–84.
- 549 Brugge, R. (2010). Forty years of the Climatological Observers Link. *Weather*, 65(5):139–143.
- 550 Chapman, L., Bell, C., and Bell, S. (2017). Can the crowdsourcing data paradigm take
551 atmospheric science to a new level? A case study of the urban heat island of London
552 quantified using Netatmo weather stations. *Int. J. Climatol.*, 37(9):3597–3605.
- 553 de Vos, L., Leijnse, H., Overeem, A., and Uijlenhoet, R. (2017). The potential of urban
554 rainfall monitoring with crowdsourced automatic weather stations in amsterdam. *Hydrology
555 and Earth System Sciences*, 21(2):765–777.

556 Deneke, H., Feijt, A., and Roebeling, R. (2008). Estimating surface solar irradiance from
557 METEOSAT SEVIRI-derived cloud properties. *Remote Sens. Environ.*, 112(6):3131–3141.

558 DESA, U. (2017). World population prospects. United Nations Department of Economic and
559 Social Affairs (UN DESA) Population Division, New York, NY, USA, revision edition.

560 Fenner, D., Meier, F., Bechtel, B., Otto, M., and Scherer, D. (2017). Urban Meteorology Intra
561 and inter 'local climate zone' variability of air temperature as observed by crowdsourced
562 citizen weather stations in Berlin, Germany. 26(5):525–547.

563 Greuell, W., Meirink, J. F., and Wang, P. (2013). Retrieval and validation of global, direct,
564 and diffuse irradiance derived from SEVIRI satellite observations. *J. Geophys. Res. Atmos.*,
565 118(5):2340–2361.

566 Haines, A., Kovats, R., Campbell-Lendrum, D., and Corvalan, C. (2006). Climate change and
567 human health: Impacts, vulnerability and public health. *Public Health*, 120(7):585–596.

568 Hastie, T. and Tibshirani, R. (1990). *Generalized additive models*. Chapman & Hall/CRC.

569 Heusinkveld, B. G., Hove van, L., Jacobs, C. M. J., Steeneveld, G. J., Elbers, J. A., Moors,
570 E. J., and Holtslag, A. A. M. (2010). Use of a mobile platform for assessing urban heat
571 stress in Rotterdam. In *Proc. 7th Conf. Biometeorol.*, pages 433–438, Freiburg, Germany.

572 Heusinkveld, B. G., Steeneveld, G. J., van Hove, L. W. A., Jacobs, C. M. J., and Holtslag, A.
573 A. M. (2014). Spatial variability of the Rotterdam urban heat island as influenced by urban
574 land use. *J. Geophys. Res. Atmos.*, 119(2):677–692.

575 Jenkins, G. (2014). A comparison between two types of widely used weather stations. *Weather*,
576 69(4):105–110.

577 Krennert, T., Pistotnik, G., Kaltenberger, R., and Csekits, C. (2018). Crowdsourcing of
578 weather observations at national meteorological and hydrological services in Europe. *Adv.*
579 *Sci. Res*, 15:71–76.

580 Li, D. and Bou-Zeid, E. (2013). Synergistic interactions between urban heat islands and
581 heat waves: the impact in cities is larger than the sum of its parts*. *Journal of Applied*
582 *Meteorology and Climatology*, 52(9):2051–2064.

583 Li, D., Sun, T., Liu, M., Yang, L., Wang, L., and Gao, Z. (2015). Contrasting responses of
584 urban and rural surface energy budgets to heat waves explain synergies between urban heat
585 islands and heat waves. *Environmental Research Letters*, 10(5):054009.

586 Lindberg, F. and Grimmond, C. S. B. (2011). The influence of vegetation and building mor-
587 phology on shadow patterns and mean radiant temperatures in urban areas: Model devel-
588 opment and evaluation. *Theoretical and Applied Climatology*, 105(3-4):311–323.

589 Meier, F., Fenner, D., Grassmann, T., Otto, M., and Scherer, D. (2017). Crowdsourcing
590 air temperature from citizen weather stations for urban climate research. *Urban Climate*,
591 19(nil):170–191.

592 Molenaar, R. E., Heusinkveld, B. G., and Steeneveld, G. J. (2016). Projection of rural and
593 urban human thermal comfort in The Netherlands for 2050. *Int. J. Climatol.*, 36(4):1708–
594 1723.

595 Muller, C. L., Chapman, L., Grimmond, C. S., Young, D. T., and Cai, X. (2013). Sensors and
596 the city: A review of urban meteorological networks. *Int. J. Climatol.*, 33(7):1585–1600.

597 Napoly, A., Grassmann, T., Meier, F., and Fenner, D. (2018). Development and application
598 of a statistically-based quality control for crowdsourced air temperature data. *Frontiers in*
599 *Earth Science*, 6(nil):nil.

600 Oke, T. R. (1982). The energetic basis of the urban heat island. *Quarterly Journal of the*
601 *Royal Meteorological Society*, 108(455):1–24.

602 Oke, T. R., Mills, G., Christen, A., and Voogt, J. A. (2017). *Urban Climates*. Cambridge
603 University Press, Cambridge.

604 Roebeling, R. A., Feijt, A. J., and Stammes, P. (2006). Cloud property retrievals for cli-
605 mate monitoring: Implications of differences between Spinning Enhanced Visible and In-
606 frared Imager (SEVIRI) on METEOSAT-8 and Advanced Very High Resolution Radiometer
607 (AVHRR) on NOAA-17. *J. Geophys. Res.*, 111(D20):D20210.

608 Ronda, R. J., Steeneveld, G. J., Heusinkveld, B. G., Attema, J. J., and Holtslag, A. A. (2017).
609 Urban finescale forecasting reveals weather conditions with unprecedented detail. *Bull. Am.*
610 *Meteorol. Soc.*, 98(12):2675–2688.

611 Steeneveld, G. J., Koopmans, S., Heusinkveld, B. G., Van Hove, L. W., and Holtslag, A. A.
612 (2011). Quantifying urban heat island effects and human comfort for cities of variable size
613 and urban morphology in the Netherlands. *J. Geophys. Res. Atmos.*, 116(20):1–14.

614 Theeuwes, N. E., Steeneveld, G.-J., Ronda, R. J., and Holtslag, A. A. M. (2016). A diagnostic
615 equation for the daily maximum urban heat island effect for cities in northwestern europe.
616 *International Journal of Climatology*, 37(1):443–454.

617 Thorsson, S., Rocklöv, J., Konarska, J., Lindberg, F., Holmer, B., Dousset, B., and Rayner,
618 D. (2014). Mean radiant temperature - a predictor of heat related mortality. *Urban Climate*,
619 10(nil):332–345.

620 van den Hurk, B., Klein Tank, A., Lenderink, G., van Ulden, A., van Oldenborgh, G. J.,
621 K. C., van den Brink, H., Keller, F., Bessembinder, J., Burgers, G., Komen, G., Hazeleger,
622 W., and Drijfhout, S. (2006). KNMI Climate Change Scenarios 2006 for the Netherlands.
623 KNMI, De Bilt.

624 WMO (2014). Guide to meteorological instruments and methods of observation.

625 Wolters, D. and Brandsma, T. (2012). Estimating the Urban Heat Island in Residential Areas
626 in the Netherlands Using Observations by Weather Amateurs. *J. Appl. Meteorol. Climatol.*,
627 51(4):711–721.

628 Wood, S. (2018). *mgcv: Mixed GAM Computation Vehicle with Automatic Smoothness Esti-*
629 *mation*.

630 Wood, S. N. (2003). Thin plate regression splines. *J. R. Stat. Soc. Ser. B (Statistical Methodol.*,
631 65(1):95–114.

632 Wood, S. N. (2006). *Generalized Additive Models: An Introduction with R*. Chapman and
633 Hall/CRC.

634 Wood, S. N., Li, Z., Shaddick, G., and Augustin, N. H. (2017). Generalized additive models
635 for gigadata: Modeling the u.k. black smoke network daily data. *Journal of the American*
636 *Statistical Association*, 112(519):1199–1210.

637 Zhao, L., Oppenheimer, M., Zhu, Q., Baldwin, J. W., Ebi, K. L., Bou-Zeid, E., Guan, K., and
638 Liu, X. (2018). Interactions between urban heat islands and heat waves. *Environmental*
639 *Research Letters*, 13(3):034003.

Table 1: Properties of the four sample stations. The Urban Climate Zone (UCZ), Temperature and Exposure are subjective assessments of the site and are supplied by the respective site operators. The UCZ is as defined by the WMO (2014) ¹ 5 - Medium development; 6 - Mixed use with large buildings in open landscape; 7 - Semi-rural development. ² A - Standard instruments in Stevenson Screen; B - Standard instruments in Stevenson Screen or manufacturer supplied AWS shortwave radiation screen; C - Standard instruments in Stevenson Screen or manufacturer supplied AWS shortwave radiation screen, site exposure 1 or less. ³ Exposure: I - Sheltered exposure; II - Restricted exposure; III - Standard exposure; V - Very open exposure.

	Longitude (°E)	Latitude (°N)	Instrument	Urban Climate Zone ¹	Instrumentation ²	Exposure ³
A	5.176	52.098	Vaisala WXT520	6	B	II
B	5.253	52.079	Davis VP2	5	C	I
C	5.294	51.396	Davis VP2	7	A	V
D	6.687	52.348	AcuRite 5-in-1	5	B	III

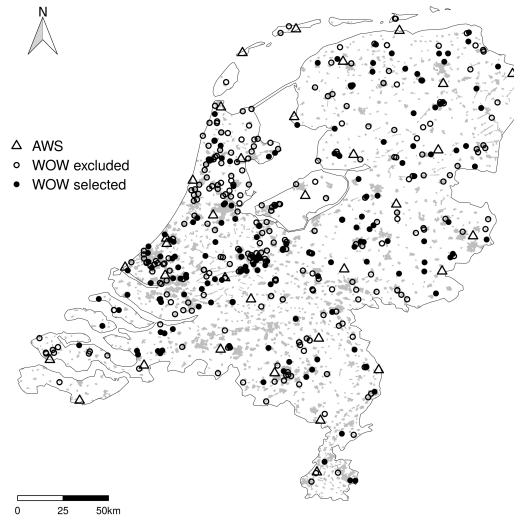


Figure 1: The locations of the official KNMI AWS and the WOW stations across the Netherlands. The WOW stations are categorized into those stations used in the study (WOW selected), and those that contained too many missing values for the models to be applied (WOW excluded). Urban areas defined using the Coordination of Information on the Environment (CORINE) land-cover dataset (CLC2018) are indicated by shading.

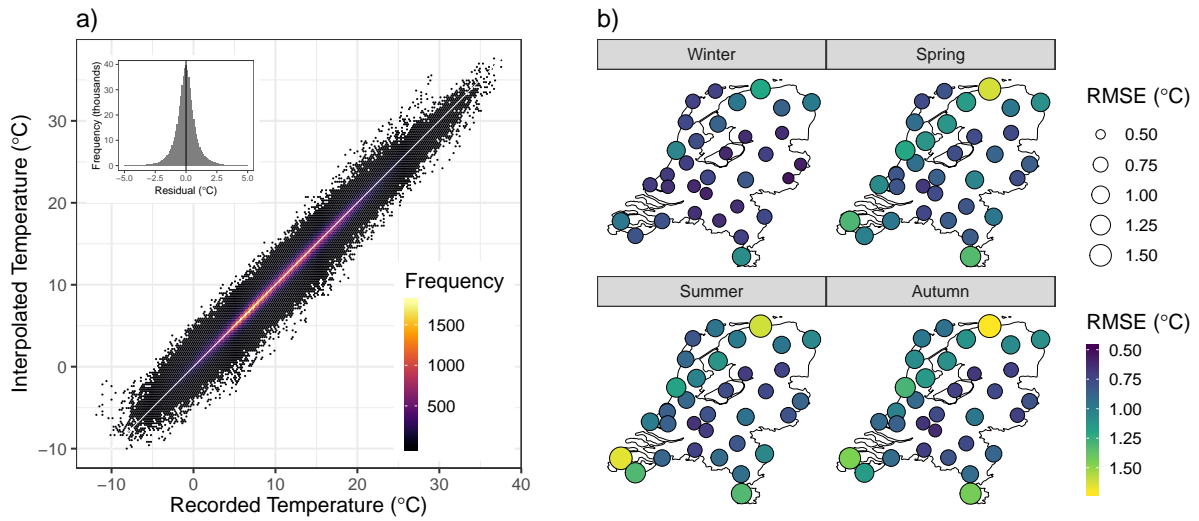


Figure 2: Results of the leave-one-out cross-validation of the KNMI temperature observations. a) shows a scatter plot of the interpolated values relative to the recorded temperature values, and b) shows the root-mean square error between the interpolated and recorded values. The inset in a) shows a histogram of the interpolated *minus* the recorded values. The seasons take the conventional meteorological definition (Winter as Dec-Feb, Spring as Mar-May etc.).

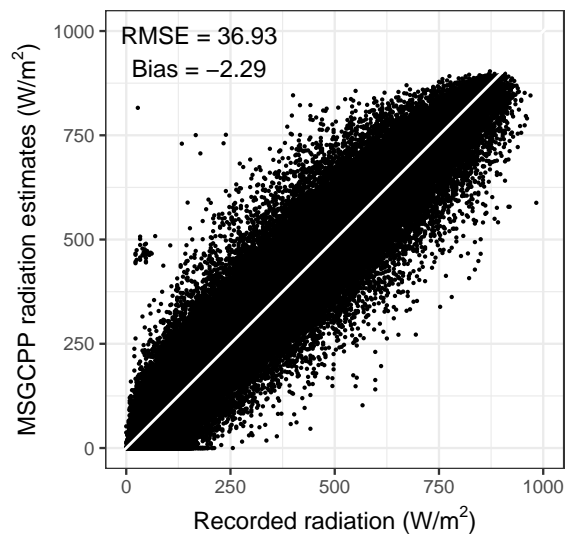


Figure 3: Hourly-mean comparison of the MSG-CPP direct shortwave radiation estimates relative to recorded shortwave radiation at the official KNMI stations over the period 2015–2016.

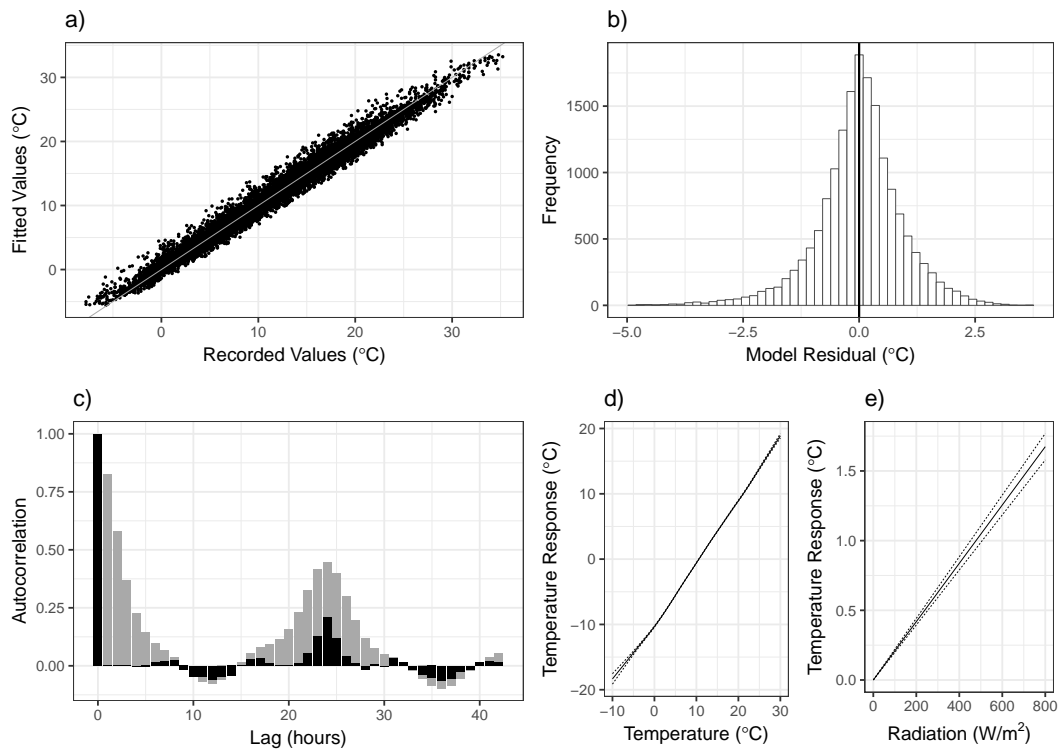


Figure 4: Plots of several model attributes for station B: a scatter plot of fitted values against predictand values (a); a histogram of the model residuals, with the vertical line indicating the mean value (b); autocorrelation function (ACF) for a GAMM with assumed lag-2 autocorrelation (black) and assuming independent residuals (grey) after Wood et al. (2017) (c); and the temperature (d) and shortwave radiation (e) partial terms from the model. In d) and e) the standard errors of the partial model terms are also indicated (dashed lines).

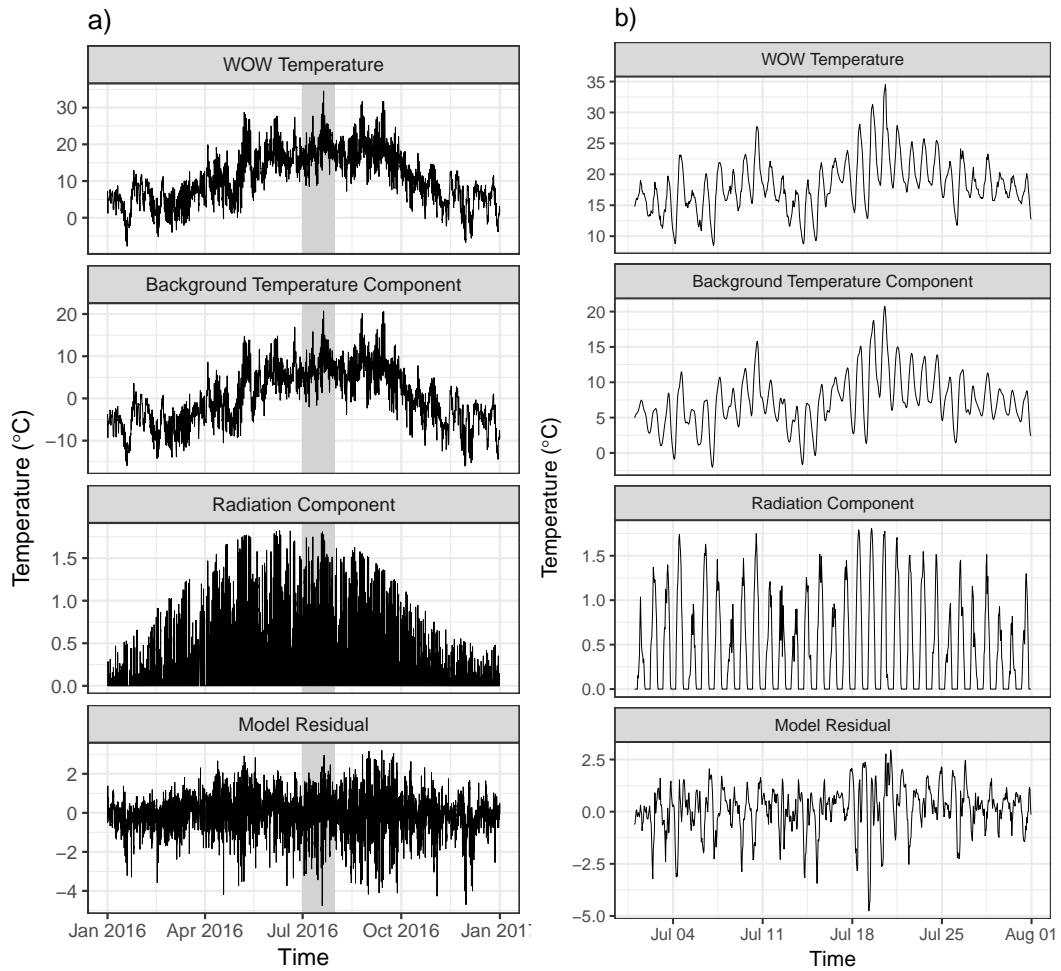


Figure 5: Time series plots showing the original WOW temperature data at test station B, the background temperature and shortwave radiation terms, and the model residual for the year 2016 (a) and for July 2016 (b). The shaded region in (a) indicates the period covered in (b). Note the slightly different y-axis scaling between (a) and (b)

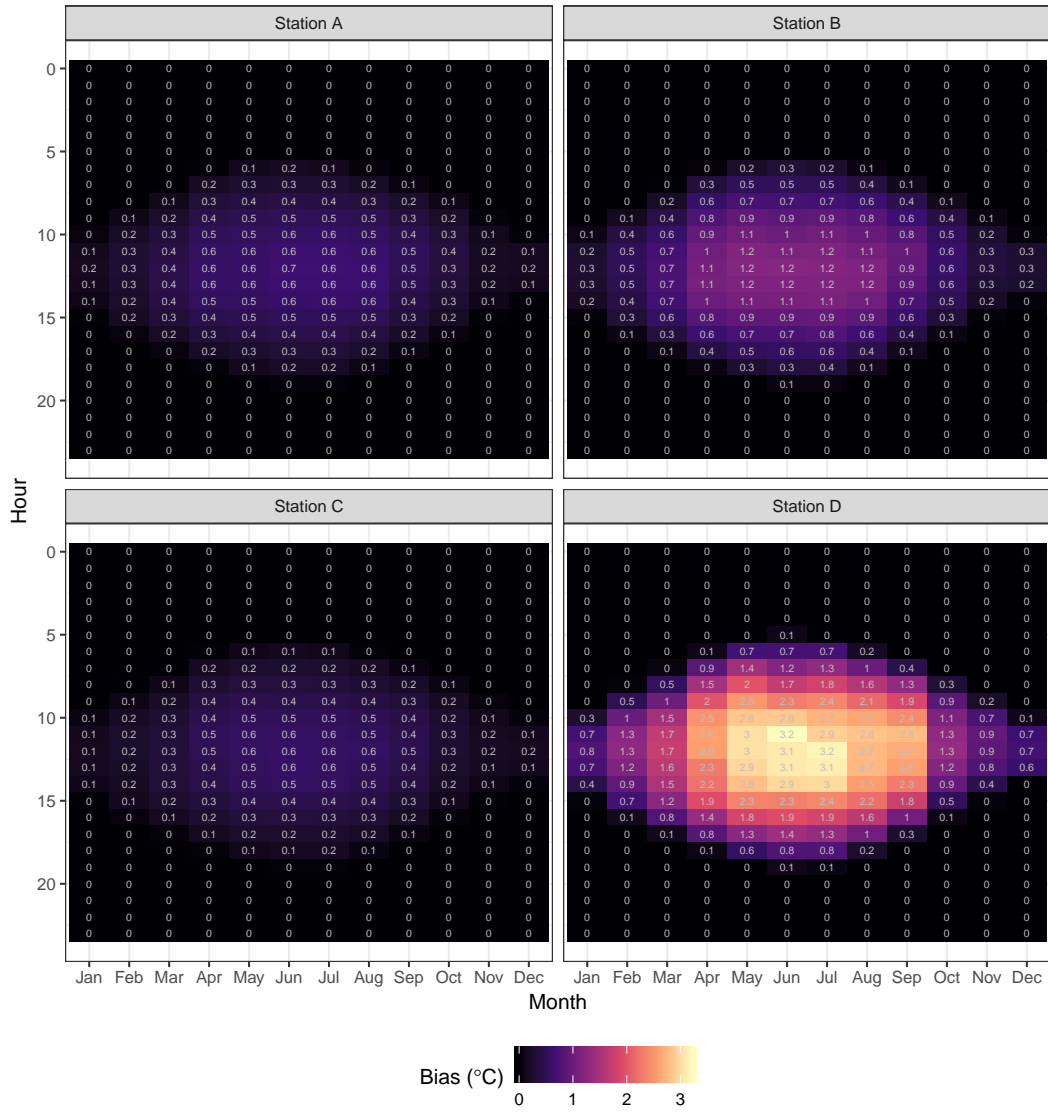


Figure 6: The estimated shortwave radiation bias ($T'_{wov,i} - T_{wov}$) for the four WOW test stations over the period 2015–2016. The plots indicate the average bias per month (x-axis) against the hour of the day (UTC, y-axis).

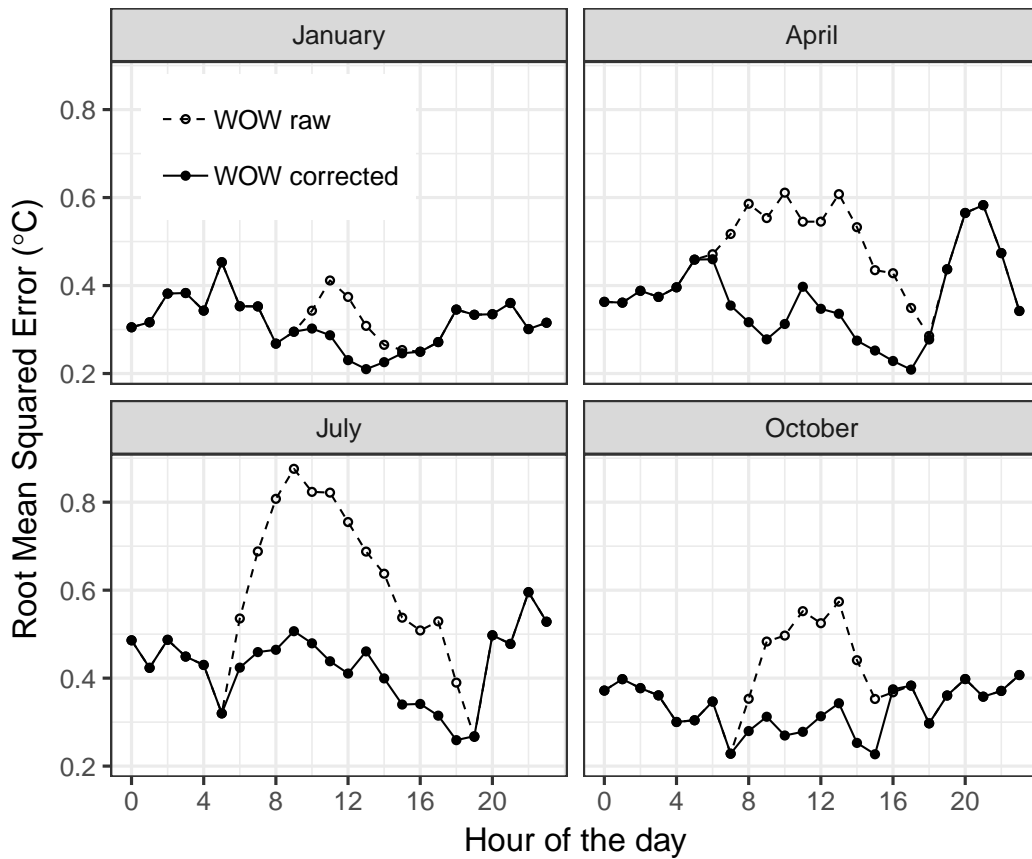


Figure 7: Root-mean squared error values of the raw and corrected WOW data at the De Bilt meteorological enclosure relative to the official AWS values over the period 2015–2016. Values are calculated for each hour of the day in the months indicated.

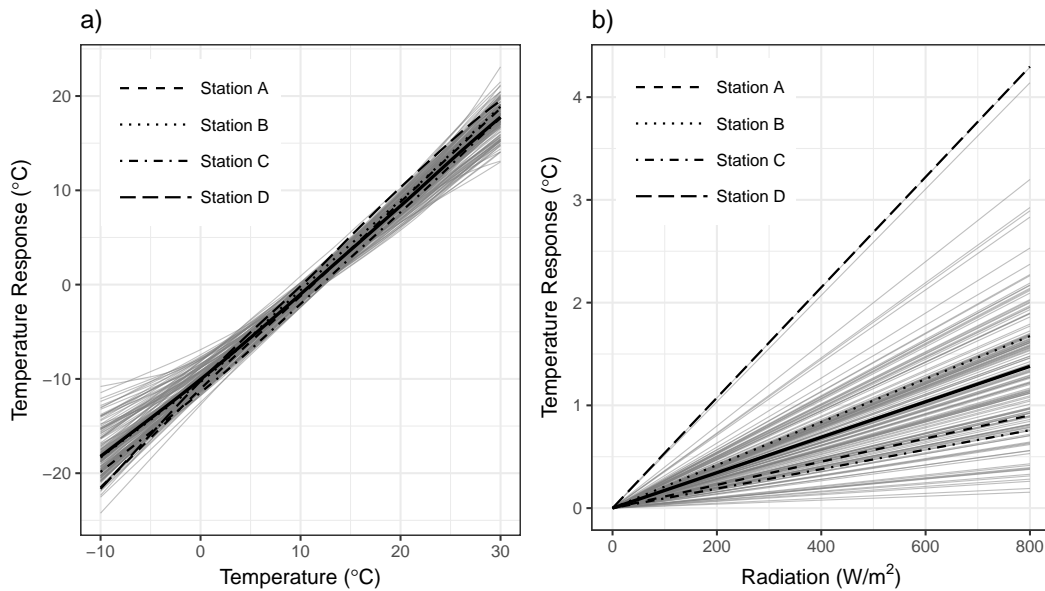


Figure 8: Plots showing the background temperature (a) and shortwave radiation (b) partial model terms calculated from the GAMMs for each WOW station (grey lines). The continuous black line indicates the mean across the station models, and the values for the four test stations are highlighted. The models are fitted using data from the full 24-month period.

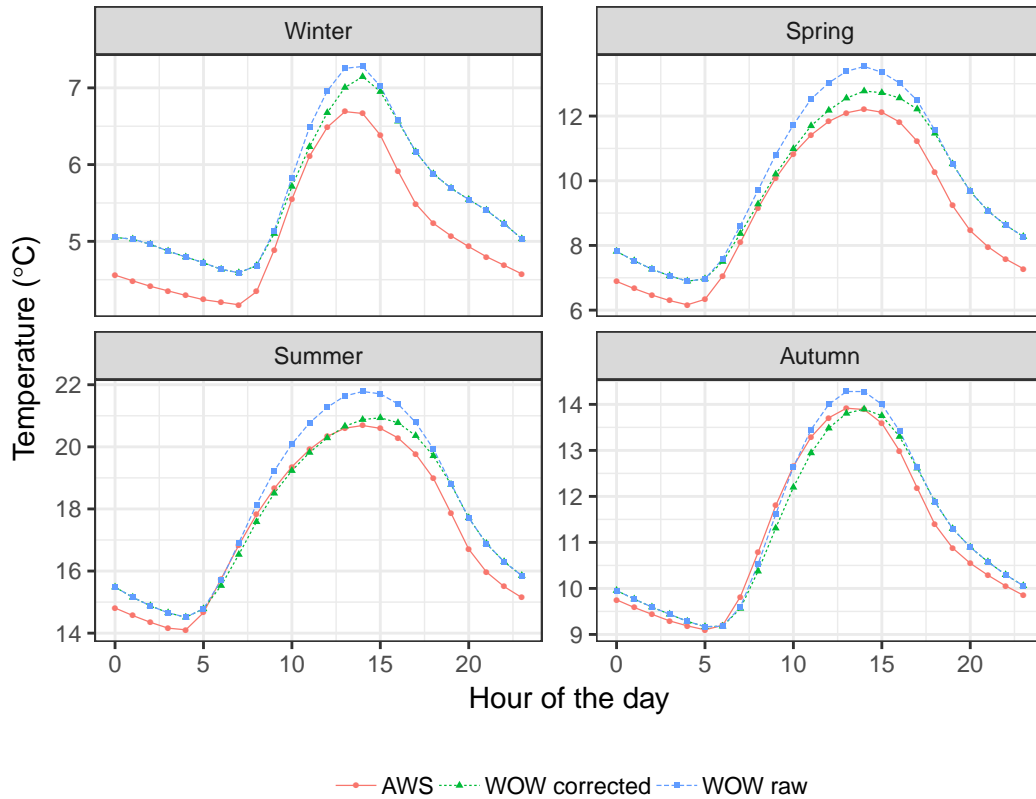
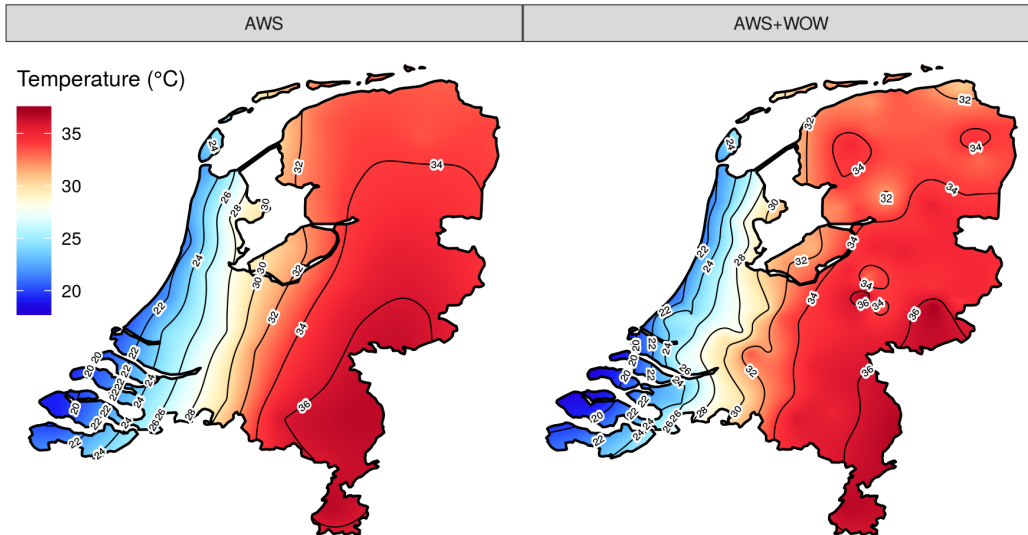


Figure 9: Average temperature values per hour of the day (UTC) over the period 2015–2016 for each season calculated as the mean from the KNMI AWS weather stations and the raw/corrected WOW stations. Note the different y-axis in each of the panels. The seasons take the conventional meteorological definition (Winter as Dec-Feb, Spring as Mar-May etc.)

a) 2015 07 02 13:00



b) 2016 01 19 03:00

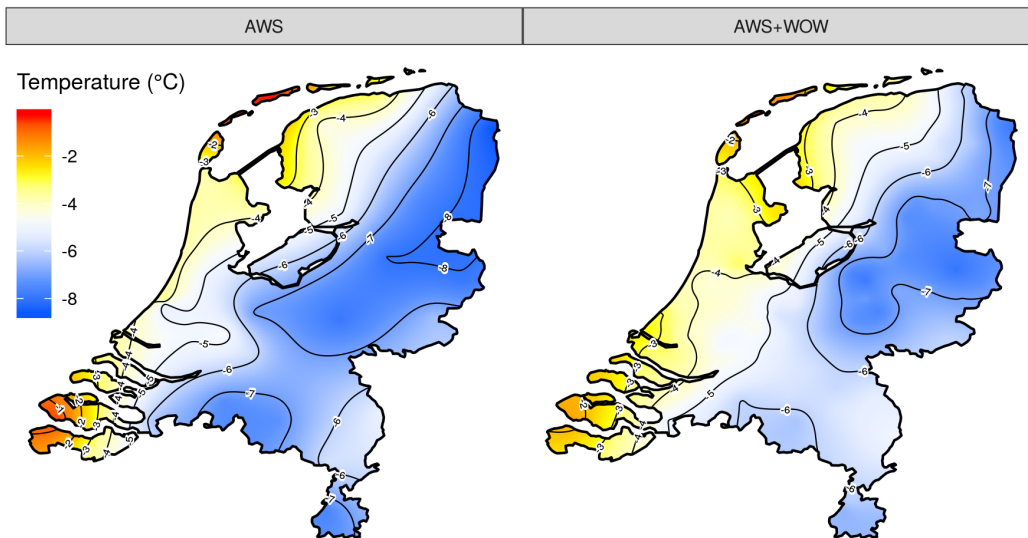


Figure 10: Maps of interpolated temperature for a) 1300 UTC on 2nd July 2015 and b) 0300 UTC on 19th January 2016. The maps on the left (AWS) are produced using only the official KNMI station readings, and the maps on the right (AWS+WOW) use both the corrected WOW temperature measurements and the AWS data. The maps are produced using ordinary kriging, with a separate variogram fitted to each map. Note the different contour spacing in a) (2 °C) compared to b) (1 °C).